**Immunity, Volume *55***

## Supplemental information

# Mechanistic convergence of the TIGIT and PD-1 inhibitory pathways necessitates co-blockade to optimize anti-tumor $CD8^+$ T cell responses

**Karl L. Banta, Xiaozheng Xu, Avantika S. Chitre, Amelia Au-Yeung, Chikara Takahashi, William E. O'Gorman, Thomas D. Wu, Stephanie Mittman, Rafael Cubas, Laetitia Comps-Agrar, Amit Fulzele, Eric J. Bennett, Jane L. Grogan, Enfu Hui, Eugene Y. Chiang, and Ira Mellman**

# Mechanistic convergence of the TIGIT and PD-1 inhibitory pathways necessitates co-blockade to optimize anti-tumor CD8+ T cell responses

Karl L. Banta[1,5], Xiaozheng Xu[2.,5], Avantika S. Chitre[1], Amelia Au-Yeung[1], Chikara Takahashi[1], William E. O'Gorman[1], Thomas D. Wu[1], Stephanie Mittman[1], Rafael Cubas[1,3], Laetitia Comps-Agrar[1], Amit Fulzele[2], Eric J. Bennett[2], Jane L. Grogan[1,4], Enfu Hui[2,6], Eugene Y. Chiang[1,6*], and Ira Mellman[1,6,7*]

[1] Genentech, Inc., 1 DNA Way, South San Francisco, CA 94080. [2] Section of Cell & Developmental Biology, Division of Biological Sciences, University of California, San Diego, 9500 Gilman Drive, La Jolla, CA 92093, [3] Present address: Iovance, 3802 Spectrum Blvd., Tampa, FL 33612, [4] Present address: Graphite Bio, 279 E. Grand Avenue, South San Francisco, CA 94080. [5] These authors contributed equally to this work. [6] Senior authors. [7] Lead contact.

[*] Corresponding authors:
Eugene Y. Chiang, email: chiang.eugene@gene.com
Ira Mellman, email: mellman.ira@gene.com; mobile: 650-452-3894

## SUPPLEMENTAL INFORMATION

**Table S1.** Patient characteristics and tumor metadata by individual for tissue samples analyzed by CyTOF and scRNAseq, Related to Figures 3 and 4.

| Sample Code | NSCLC1 | NSCLC2 | NSCLC3 | NSCLC4 | NSCLC5 | NSCLC6 |
|---|---|---|---|---|---|---|
| Matched scRNAseq | NA | NA | NA | Y | Y | Y |
| Tumor Indication | NSCLC | NSCLC | NSCLC | NSCLC | NSCLC | NSCLC |
| Age | 72 | 83 | 51 | 60 | 55 | 67 |
| Gender | F | M | M | F | M | F |
| Ethnicity | White | White | White | White | White | White |
| Tumor Stage | Ia | IIa | III | I | III | Not Available |
| Histology Subtype | Adenocarcinoma | Squamous Cell Carcinoma | Squamous Cell Carcinoma (Keratinizing) | Squamous Cell Carcinoma (Nonkeratinizing) | Not Available | Not Available |
| T (Area of Cancer) | T1b | T2b | T2a | T2a | T4 | Not Available |
| N (Lymph Node Spread) | N0 | N0 | N2 | N0 | N1 | Not Available |
| M (Metastasis) | MX | MX | MX | MX | MX | Not Available |

**Table S2.** Antibodies used for CyTOF panel to phenotype tumor immune cell infiltrate, Related to Figure 3.

| Mass | Metal | Target | Source | Vendor | Clone | Catalog Number | Lot Number |
|---|---|---|---|---|---|---|---|
| 89 | Y | CD45 | Fluidigm | | HI30 | 3089003B | 2291710 |
| 113 | In | EpCAM | Custom | Biolegend | 9C4 | | In-house |
| 115 | In | CD57 | Custom | Biolegend | HCD57 | | In-house |
| 140 | Ce | EQ Beads | | | | | |
| 141 | Pr | Perforin | Custom | Abcam | B-D48 | | In-house |
| 142 | Nd | CCR4 | Custom | R&D | 205410 | | In-house |
| 143 | Nd | CD127/ CD137/CCR8 | Fluidigm/ Custom | Biolegend | A019D5/ 4B4-1/ L263G8 | 3143012B | 2191516 In-house |
| 144 | Nd | Granzyme B | Custom | Biolegend | GB11 | | In-house |
| 145 | Nd | CD4 | Fluidigm | | RPA-T4 | 3145001B | 1931719 |
| 146 | Nd | CD8 | Fluidigm | | RPA-T8 | 3146001B | 1671716 |
| 147 | Sm | CD11c | Fluidigm | | Bu15 | 3147008B | 0731704 |
| 148 | Nd | CD56 | Custom | Miltenyi | REA196 | | In-house |
| 149 | Sm | Granzyme A | Custom | Biolegend | CB9 | | In-house |
| 150 | Nd | CD103 | Custom | Biolegend | Ber-ACT8 | | In-house |
| 151 | Eu | ICOS | Custom | eBioscience | ISA-3 | | In-house |
| 152 | Sm | CD155 PVR/ CD39 | Custom | Biolegend | SKII.4/ A1 | | In-house |
| 153 | Eu | TIM3 | Custom | R&D | 344823 | | In-house |
| 154 | Sm | CD3 | Fluidigm | | UCHT1 | 3154003B | 1351723 |
| 155 | Gd | CD27 | Fluidigm | | L128 | 3155001B | 1031712 |
| 156 | Gd | CXCR3 | Fluidigm | | G025H7 | 3156004B | 1681613 |
| 157 | Gd | CD14 | Custom | | M5E2 | | In-house |
| 158 | Gd | OX40 | Custom | Genentech | 1A7.gr.1 | | In-house |
| 159 | Tb | CD226 | Custom | BD | DX11 | | In-house |
| 160 | Gd | Tbet | Fluidigm | | 4B10 | 3160010B | 1061601 |
| 161 | Dy | CTLA4 | Custom | Biolegend | BNI3 | | In-house |
| 162 | Dy | Foxp3 | Fluidigm | | PCH101 | 3162011A | 0731702 |
| 163 | Dy | Eomes | Custom | eBioscience | WD1928 | | In-house |
| 164 | Du | CD161 | Fluidigm | | HP-3G10 | 3164009B | 3271610 |
| 165 | Ho | CD19 | Fluidigm | | HIB19 | 3165025B | 3121611 |
| 166 | Er | NKG2D | Fluidigm | | ON72 | 3166016B | 0091703 |
| 167 | Er | CCR7 | Fluidigm | | G043H7 | 3167009A | 0241815 |
| 168 | Er | Ki-67 | Fluidigm | | Ki-67 | 3168007B | 0861703 |
| 169 | Tm | CD25 | Fluidigm | | 2A3 | 3169003B | 1931713 |
| 170 | Er | CD45RA | Fluidigm | | HI100 | 3170010B | 0981521 |
| 171 | Yb | PD-L1 | Custom | Genentech | 14D3 | | In-house |
| 172 | Yb | CD28 | Custom | Biolegend | CD28.2 | | In-house |
| 173 | Yb | TIGIT | Fluidigm | | MBSA43 | 3999999-5 | 1461701 |
| 174 | Yb | HLA-DR | Fluidigm | | L243 | 3174001B | 0041719 |
| 175 | Lu | PD-1 | Fluidigm | | EH12.2H7 | 3175008B | 2431709 |
| 176 | Yb | CD38 | Custom | Biolegend | HIT2 | | In-house |
| 191 | Ir | Nucleic acid | Fluidigm | | | 201192A | 2451506A |
| 192 | Pt | Cisplatin | Fluidigm | | | 201064 | 0671809 |
| 193 | Ir | Nucleic acid | Fluidigm | | | 201192A | 2451506A |
| 195 | Pt | Cisplatin | Fluidigm | | | 201064 | 0671809 |
| 209 | Bi | CD16 | Fluidigm | | 3G8 | 3209002B | 2031601 |

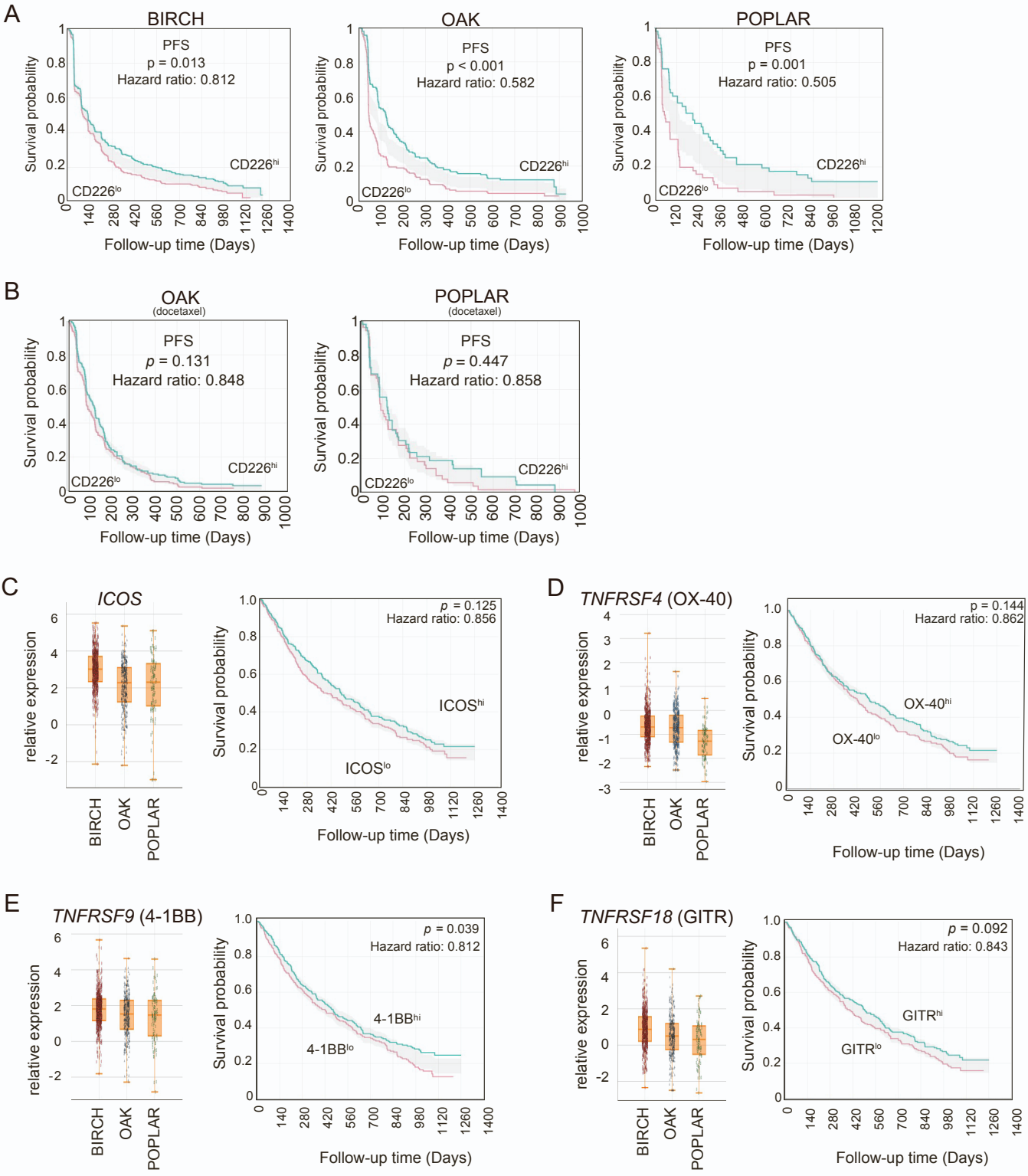


**Figure S1.** CD226 gene expression is associated with progression-free survival (PFS) in NSCLC with clinical response to atezolizumab but not docetaxel, and association of activating receptors with response to atezolizumab, Related to Figure 2.

**Figure S1.** CD226 gene expression is associated with progression-free survival (PFS) in NSCLC with clinical response to atezolizumab but not docetaxel, and association of activating receptors with response to atezolizumab, Related to Figure 2.
(A-B) Kaplan-Meier plots of PFS are shown for the atezolizumab arm (A) or docetaxel arm (B) in the indicated clinical trial. (C-F) Left panel, relative gene expression of *ICOS* (C), *TNFRSF4* encoding OX-40 (D), *TNFRSF9* encoding 4-1BB (E), and *TNFRSF18* encoding GITR (F) in BIRCH, OAK or POPLAR. Right panel, Kaplan-Meier plots of OS for indicated costimulatory markers are shown for BIRCH of the atezolizumab trials. In all plots, patients were separated on the basis of indicated gene expression into high (green line) or low (red line) expression relative to the median expression over all patients in the corresponding clinical trial. Two-sided p-values and hazard ratios from a Cox proportional hazards model are indicated for each plot.

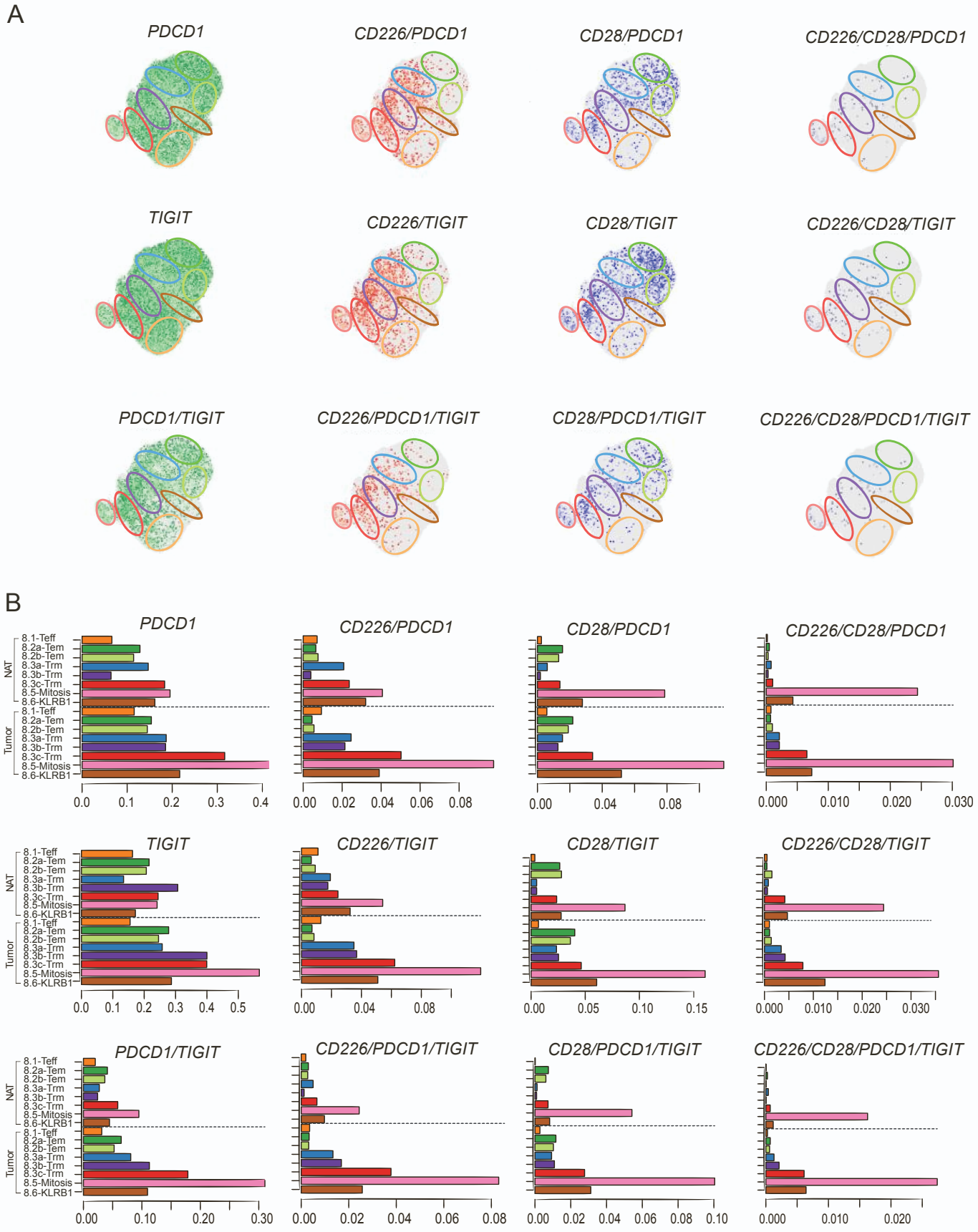


**Figure S2.** Expression of CD226, CD28, PD-1, and TIGIT by scRNA-seq in NSCLC tumors, Related to Figure 4.

**Figure S2.** Expression of CD226, CD28, PD-1, and TIGIT by scRNA-seq in NSCLC tumors, Related to Figure 4.
(A) Presence of expression for an indicated gene or gene combination of individual $CD8^+$ T cells are plotted within each UMAP overlay from Figure 4A. Labeled ovals demarcate approximate regions of the clusters. (B) Frequency of individual gene or gene combination of *CD226*, *CD28*, *PD-1,* and/or *TIGIT* within each $CD8^+$ T cell cluster are plotted by bar graph.

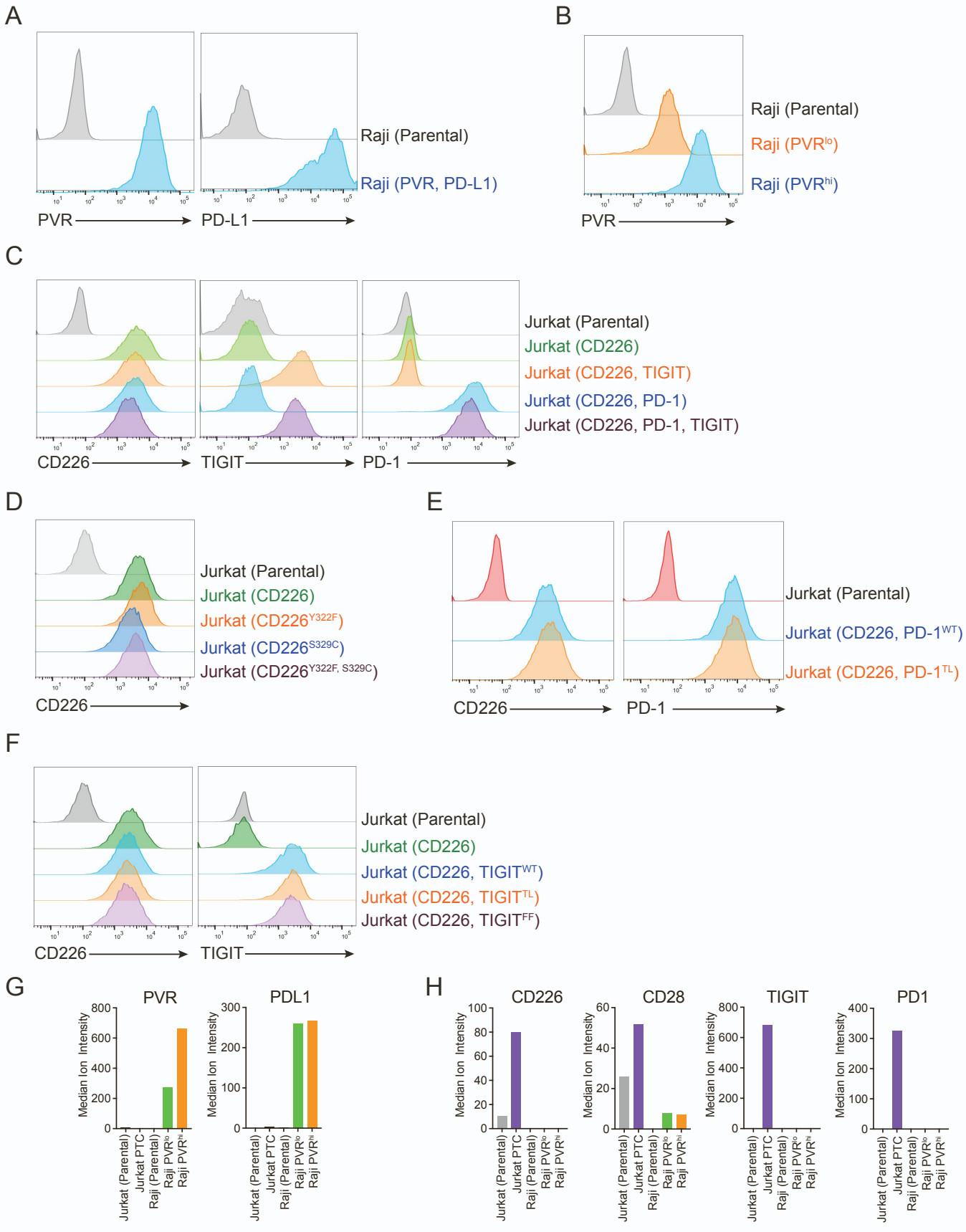


**Figure S3.** Receptor and ligand expression profiles on cell lines used in co-culture assays, Related to Figures 5 and 6.

**Figure S3.** Receptor and ligand expression profiles on cell lines used in co-culture assays, Related to Figures 5 and 6.

(A-F) Representative flow cytometry histograms showing surface expression levels of PVR, PD-L1 in Raji cells or CD226, TIGIT, and/or PD-1 in Jurkat cells. (A) Expression of PVR and PD-L1 in Raji cells. (B) Profile of $PVR^{lo}$ and $PVR^{hi}$ expressing Raji cells. (C) CD226, TIGIT and PD-1 expression in Jurkat cells. (D) Expression of WT CD226 or a Y322F, S329C, or both mutants within the CD226 protein in Jurkat cells. (E) Expression of PD-1 or $PD\text{-}1^{\Delta ICD}$ in Jurkat cells. (F) Co-expression of WT TIGIT or TIGIT mutant constructs with CD226 in Jurkat cells. The $TIGIT^{\Delta ICD}$ mutant is devoid of an intracellular tail, while $TIGIT^{FF}$ contains both critical tyrosine residues mutated to phenylalanine within the ICD . (G,H) CyTOF analysis of surface expression levels of the ligands PVR and PD-L1 (G) or the receptors CD226, CD28, TIGIT, and PD-1 (H) on Raji or Jurkat cell lines. Jurkat PTC denotes Jurkat cells transfected with PD-1, TIGIT and CD226.

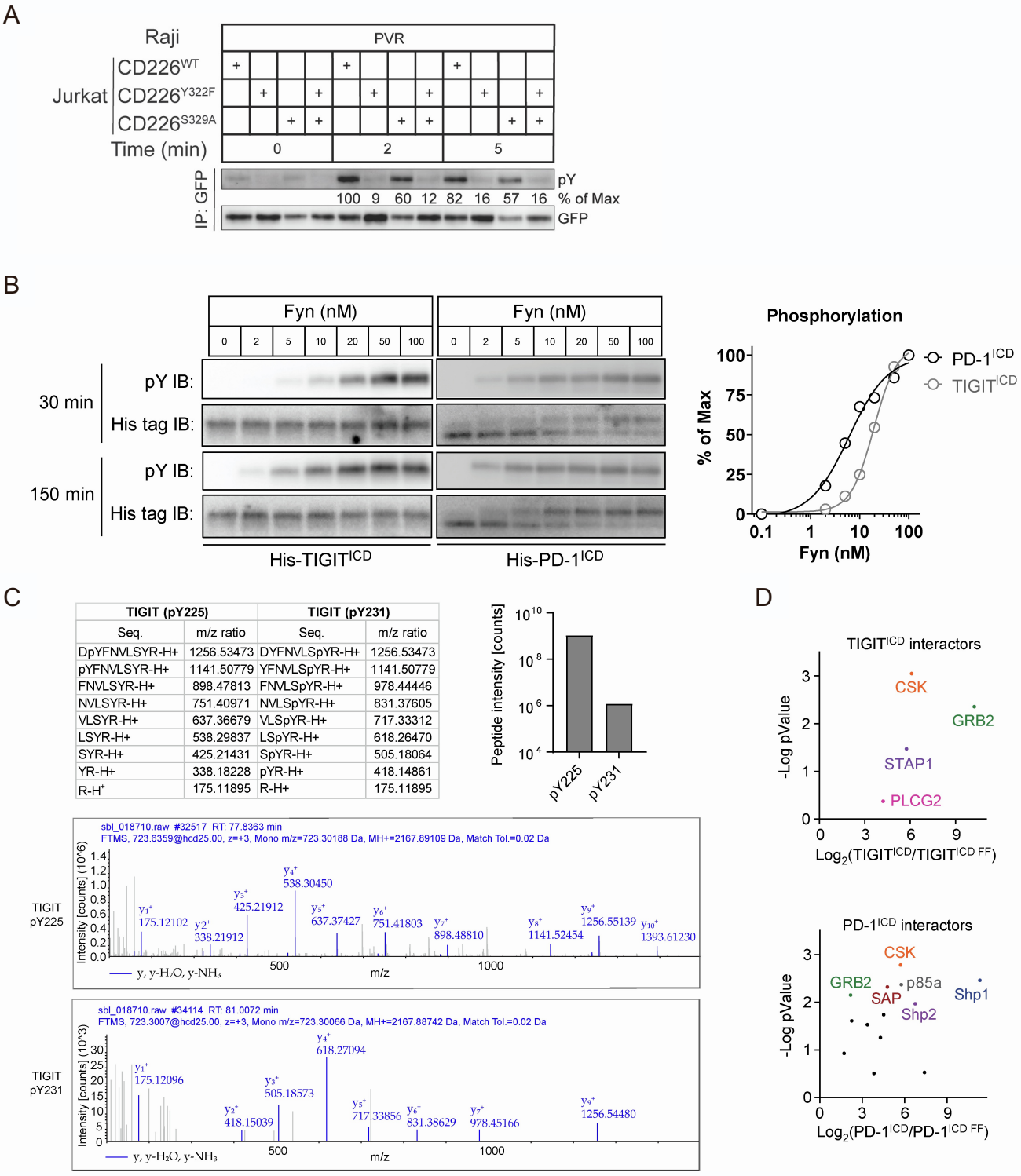


**Figure S4.** Preferential phosphorylation of CD226 is at Y322 upon PVR stimulation, and TIGIT$^{ICD}$ tends to be mono-phosphorylated at the ITT motif and failed to recruit Shp1 or Shp2, Related to Figure 5.

**Figure S4.** Preferential phosphorylation of CD226 is at Y322 upon PVR stimulation, and TIGIT$^{ICD}$ tends to be mono-phosphorylated at the ITT motif and failed to recruit Shp1 or Shp2, Related to Figure 5.

(A) pY IB showing the phosphorylation status of CD226 WT or indicated mutants using after co-culturing Jurkat cells expressing GFP-tagged CD226$^{WT}$, CD226$^{Y322F}$, CD226$^{S329A}$, or CD226$^{Y322F/S329A}$ with SEE-loaded Raji cells expressing PVR. Cells were lysed at the indicated time points after initial contact. “% of max” denotes relative phospho-CD226 levels, normalized to the band with the highest OD. (B) Left, pY IBs showing the phosphorylation of TIGIT$^{ICD}$ and PD-1$^{ICD}$ as a function of increasing Fyn concentrations. Right, ODs of pY signals, normalized to the highest OD, plotted against Fyn concentration, and fitted with a “Dose-Response-Stimulation” function using Graphpad Prism 8.0. (C) Top left, table summarizing the theoretical m/z (mass/charge) ratios of MSII ions of TIGIT$^{ICD}$ Y225 and Y231 containing peptides. Top right, bar graph showing the intensity (spectral counts) of the most abundant peptide containing pY225 or pY231. Lower, mass spectral data showing the measured m/z ratios of Y225 phosphorylated peptide, and Y231 phosphorylated peptide of TIGIT$^{ICD}$ identified in the GST-TIGIT$^{ICD}$ pull down sample using MS. (D) One-side volcano plot showing MS-identified SH2-containing proteins in GST-TIGIT$^{ICD}$ or GST-PD-1$^{ICD}$ pull down samples (see Methods). Each dot represents a single SH2-containing protein.

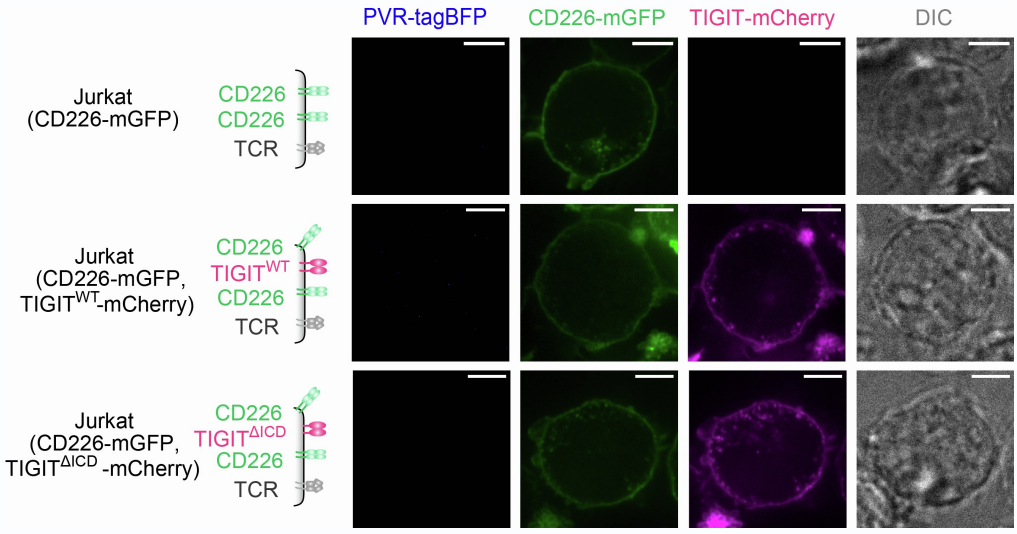


**Figure S5.** Experimental controls for the Jurkat-Raji cell conjugate assay, Related to Figure 6.

Representative confocal and DIC images of Jurkat T cells expressing CD226-GFP (top row), CD226-GFP with WT TIGIT-mCherry (middle row), or CD226-GFP with TIGIT$^{\Delta ICD}$-mCherry (bottom row) in the absence of Raji cells.

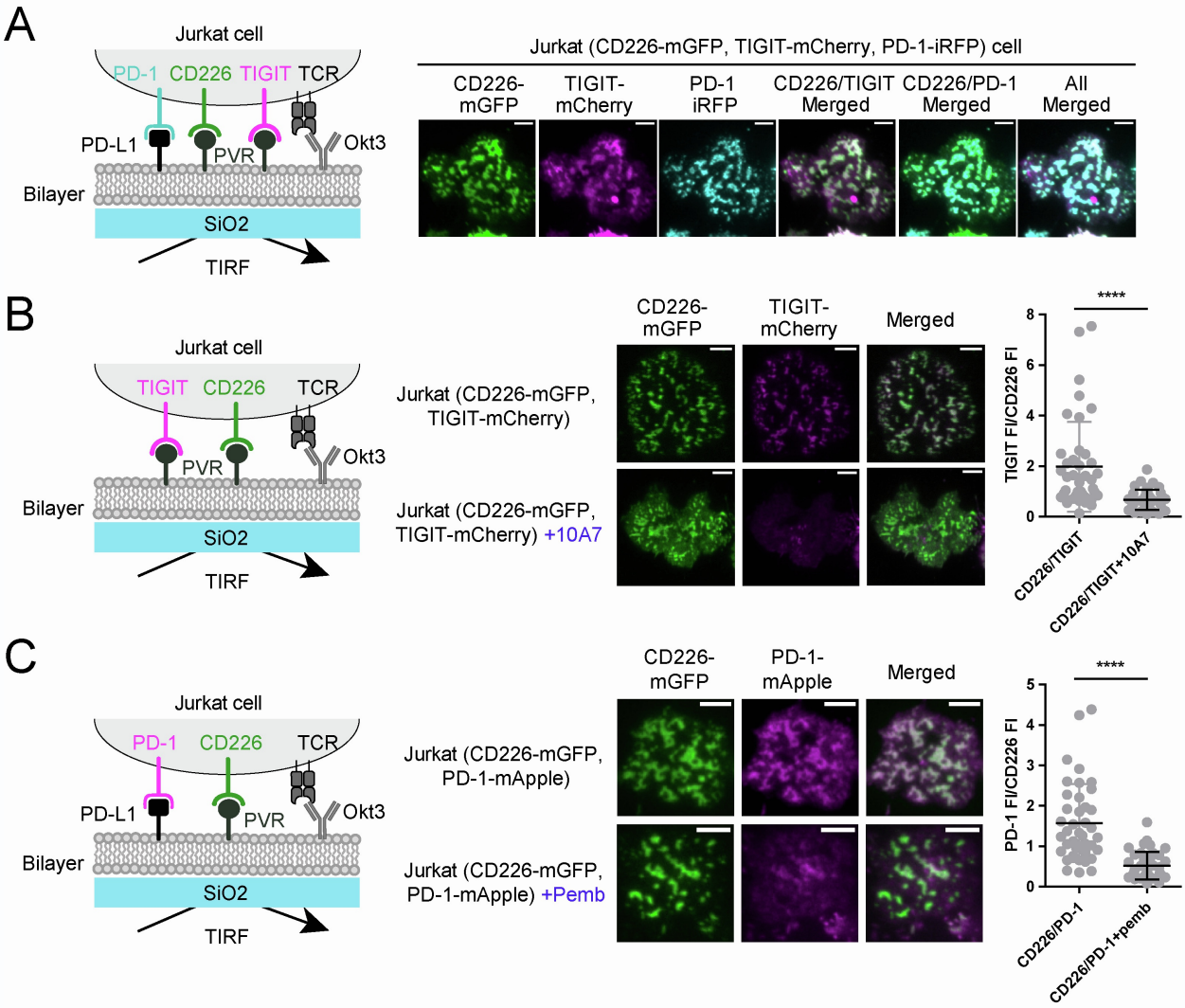


**Figure S6.** TIGIT and PD-1 both co-localize with CD226 in a ligand-dependent manner, Related to Figure 6.

(A) Left, cartoon depicting a CD226-mGFP/TIGIT-mCherry/PD-1-iRFP triple positive Jurkat cell in contact with an SLB functionalized with anti-CD3ε (clone OKT3), $PVR^{ECD}$ and $PD\text{-}L1^{ECD}$. Right, representative TIRF images showing CD226, TIGIT, and PD-1 microclusters of a single Jurkat cell. (B) Cartoon depicting a CD226-mGFP/TIGIT-mCherry double positive Jurkat cell in contact with an SLB functionalized with anti-CD3ε (clone Okt3) and $PVR^{ECD}$. Middle, representative TIRF images of CD226 and TIGIT microclusters in a Jurkat cell pretreated by PBS or by a PVR-blocking anti-TIGIT mAb (clone 10A7). Right, dot plots summarizing TIGIT FI-mCherry/CD226-mGFP FI ratios of 40 Jurkat cells under each condition (see Methods). (C) Cartoon depicting a CD226-mGFP/PD-1-mApple double positive Jurkat cell in contact with an SLB functionalized anti-CD3ε (clone Okt3), $PVR^{ECD}$ and $PD\text{-}L1^{ECD}$. Middle, representative TIRF images showing CD226 and PD-1 microclusters in a Jurkat cell pretreated by PBS or by pembrolizumab, a PD-L1 blocking anti-PD-1 mAb. Right, dot plots summarizing PD-1-mApple FI/CD226-mGFP FI ratios of 40 Jurkat cells under each condition (see Methods). Error bars: s.d.. Scale bars: 5 μm. ****P < 0.001; Student's t-test.